

Figure S1. Synaptic changes in prion-infected mice.

a, Representative electron micrographs of the stratum radiatum in the CA1 region of the hippocampus from prion-infected mice. Synapses (indicated by yellow arrowheads) are scored by the presence of synaptic vesicles presynaptically, a synaptic cleft and postsynaptic density (PSD). Scale bar: 0.5 μ m **b**, The synaptic proteins VAMP2 and NMDAR1 decline significantly at 9 w.p.i. in prion-infected mice. Representative western blots are shown. Bar graphs show quantitation compared to GAPDH loading control. **c**, qPCR data for *SNAP-25*, *VAMP2*, *NMDAR1*, *PSD-95* mRNAs at 9 and 10 w.p.i. There is no change in mRNA levels until 10 w.p.i. when neuronal numbers decline. $n = 3$ mice, repeated in triplicate. Bars represent mean \pm s.e.m. One-way ANOVA with Tukey's post test was used for multiple comparisons; $p < 0.05^*$; $p < 0.005^{**}$; $p < 0.0001^{***}$. **d**, Haematoxylin and eosin (H&E) stained sections from prion-infected mice show evolution of spongiform change and neuronal loss throughout the course of prion disease. Scale bar: 50 μ m. **e**, Amplitude (top) and decay histograms (bottom) showing fewer events per recorded neuron from prion-infected mice, with unchanged mean amplitudes and decay kinetics from whole cell recordings. Control mice were injected with normal brain homogenate (NBH) and examined at each time point. Data from controls at all time points was averaged or a representative image is shown, due to lack variability over the time course, to simplify figures.

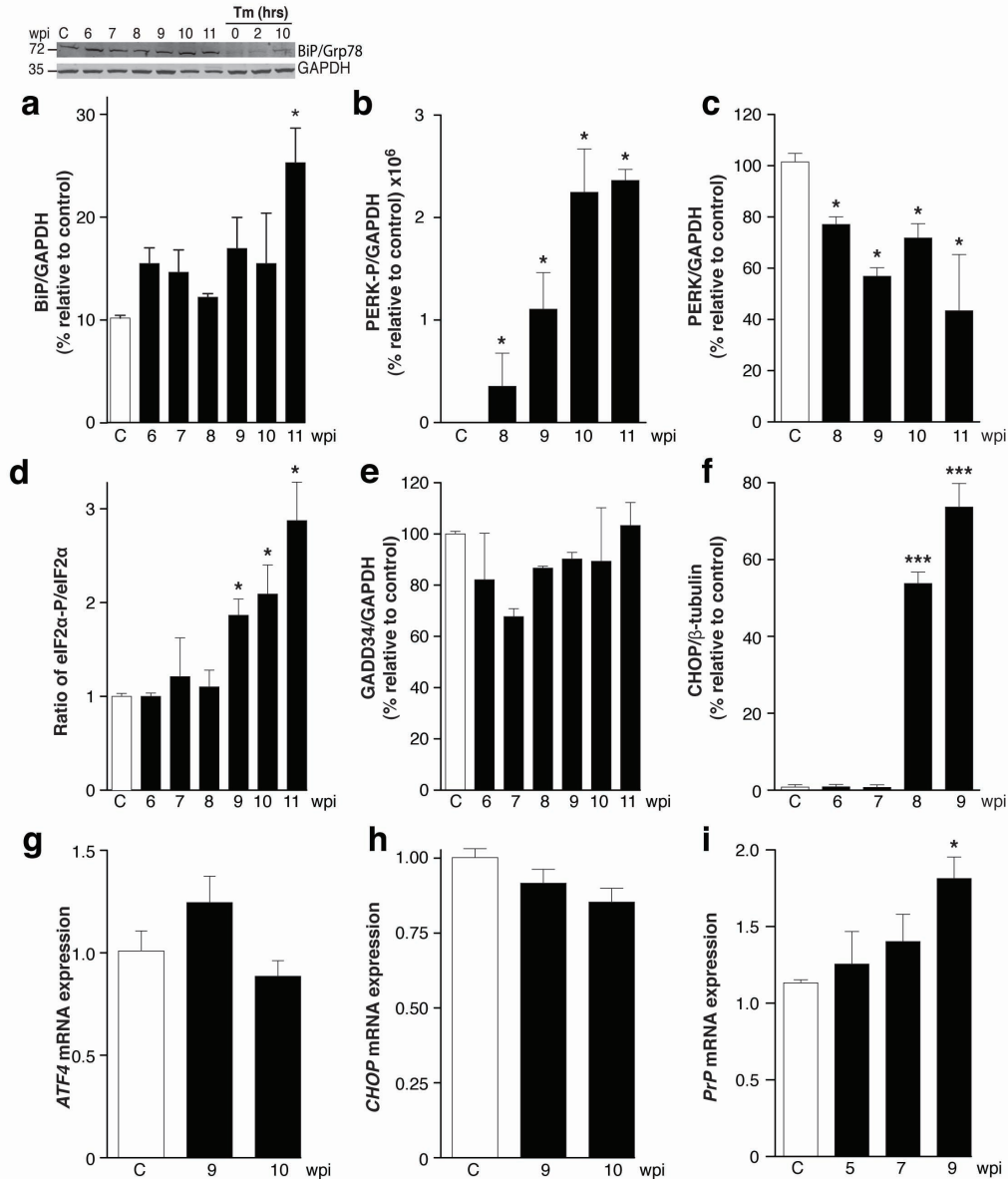


Figure S2. Quantification of proteins and mRNAs in the eIF2 α translational repression pathway during prion disease. **a**, BiP levels rise modestly towards end-stage prion disease. Representative western blots and bar chart showing quantification. **b**, and **c**, PERK-P levels rise significantly as disease evolves, with corresponding decline in PERK. No PERK-P is detected in control mice. **d**, There is a significant rise eIF2 α -P relative to eIF2 α in prion-infected mice at 9 w.p.i.; **e**, GADD34 levels do not significantly change over the course of prion disease, but **f**, CHOP levels increase at 9 w.p.i. consistent with eIF2 α -P activation. Controls are the 11 w.p.i. time point on western blots, $n = 3$ mice. **g-h**, qPCR results for *ATF4*, *CHOP* and *PrP* mRNAs. For all mRNA experiments $n = 3$ mice, repeated in triplicate. Data in bar charts represents mean \pm s.e.m. One-way ANOVA with Tukey's post test was used for multiple comparisons; $p < 0.05^*$; $p < 0.0001^{***}$.

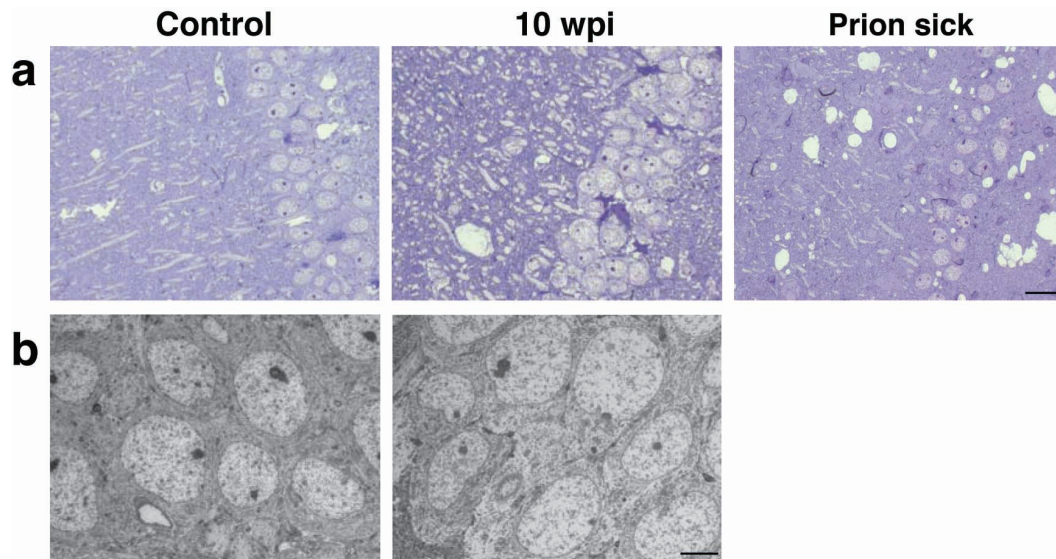


Figure S3. Cell death in prion disease. Swollen pyramidal neurons atypical of apoptosis, autophagy or necrosis are seen in prion-diseased mice. **a**, Semi-thin sections of the CA1 region of the hippocampus from which electron micrographs are taken show swollen and degenerating neurons at 10 w.p.i. and extensive neuronal loss in prion sick mice. Scale bar: 50 μ m. **b**, Electron micrographs of swollen neurons at 10 w.p.i. compared to controls. Scale bar: 5 μ m. Controls are from the 11 w.p.i. time point.

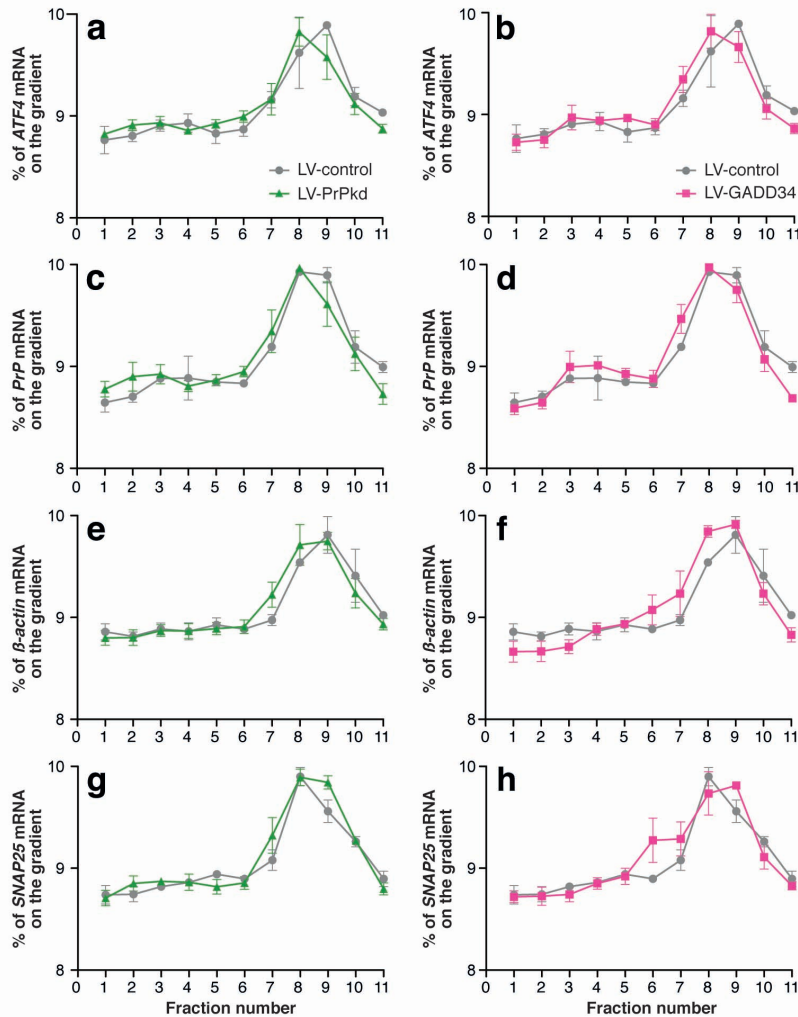


Figure S4. Quantification of specific mRNAs in individual fractions from polysomal gradients from hippocampi of LV-shPrP and LV-GADD34 treated prion-infected mice confirm reversal of activation of eIF α -P translational repression. mRNAs were quantitated in Northern blots on individual polysomal fractions from prion-infected LV-shPrP treated (green) or LV-GADD34 treated (pink), compared to LV-control treated (grey) controls, **a – h**. A shift in the peak of the curve to the right, as for *SNAP25*, is due to highest proportion of this mRNA occurring in a higher fraction where it is associated with more ribosomes, signifying a large increase in translation of these proteins in treated mice compared to LV-control treated controls at 9 w.p.i., consistent with eIF2 α -P repression. A shift in the peak of the curve to the left, as for *ATF4*, is due to the highest proportion of the mRNA being found in a lower fraction, where it is associated with fewer ribosomes, signifying a large decrease in translation, also consistent with inhibition of eIF2 α -P, which normally induces ATF4. Thus preventing eIF2 α -P formation by LV-shPrP (**a,c,e,g**) or driving its dephosphorylation via GADD34 over-expression (**b,d,f,h**) similarly affect translation. For all experiments $n = 3$ mice. Data in bar charts represents mean \pm s.e.m.

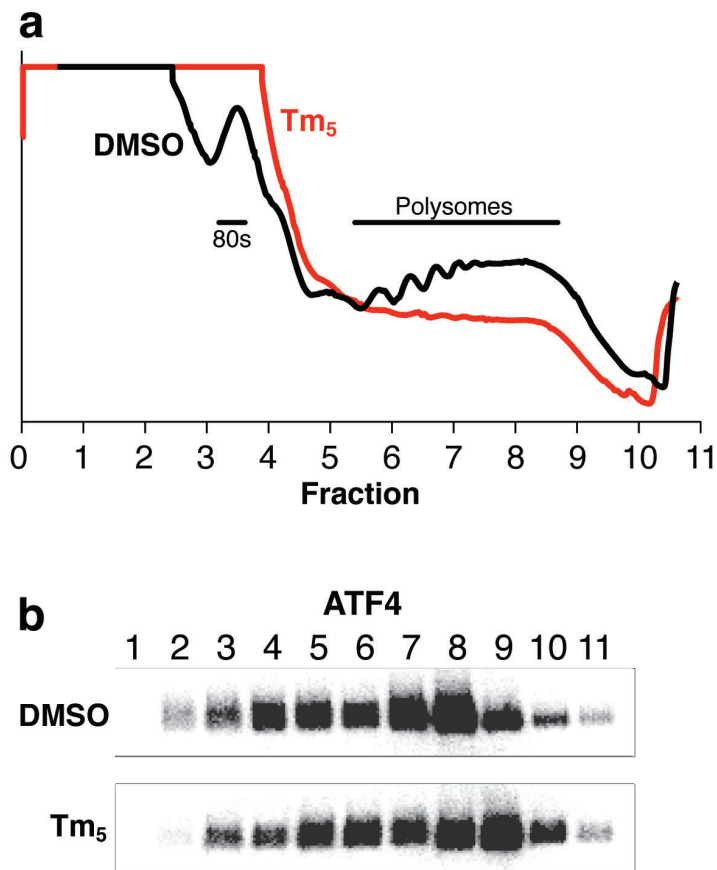


Figure S5. Tunicamycin, an ER stressor, induces eIF2 α -P-mediated changes in translation in HeLa cells. **a**, Polysomal profiles from HeLa cells treated with tunicamycin (Tm) (red) and from control cells treated with DMSO (black) show reduction in active polysomes (fractions 6-11) in Tm-treated cells. Thus the area under the Tm curve is lower than under the DMSO curve, representing reduced numbers of actively translating polysomes. This is consistent with translational repression by activation of eIF2 α -P by Tm. In contrast, eIF2 α -P induces ATF4, which is resistant to translational repression. **b**, Northern blots for *ATF4* mRNA in individual polysomal fractions from Tm treated cells show that proportionately more *ATF4* mRNA is in fractions 9 and 10 after Tm treatment for 5 hours, compared to the majority being in fractions 7 and 8 after DMSO treatment. In each successive fraction the mRNA is associated with 5-8 more ribosomes, representing a large increase in translation when mRNA is more represented in the higher fractions. $n = 3$; Northern blots were repeated in triplicate.

ATTAAGATGATTTTTACAGTCAATGAGCCACGTCAGGGAGCGATGACACCCGAGGCGGTATCAACTG
 ATGCAAGTGTTC AAGCGAATCTCAACTCGTTTTTTCCGGTGACTCATTC CCGGCCCTGCTTGGCAGCG
 TGACCCCTTTAACTTAAACCTCGGCCGGCCGCCCGGGGGCACAGAGTGTGCGCCGGGCCGCGCGG
 AATTGGTCCCCGCGCCGACCTCCGCCCGGAGCGCCGCGCTTCCCTTCCCCGCCCGCGTCCCTCCCC
 CTCGGCCCCGCGCTCGCTGTCTCCGAGCCAGTCGCTGACAGCCGCGGCCGCGAGCTTCTCCTCT
 CCTCAGACCGAGGCGAGAGCAGTCATTATGGCGAACCTTGGCTGCTGGATGCTGGTTCTCTTTGTGGCC
 ACATGGAGTGACCTGGGCCCTTGCAAGAAGCGCCCGAAGCCTGGAGGATGGAACACTGGGGGCAGCCGA
 TACCCGGGGCAGGGCAGCCCTGGAGGCAACCGCTACCCACCTCAGGGCGGTGGTGGCTGGGGGCAGCCT
 CATGGTGGTGGCTGGGGCAGCCTCATGGTGGTGGCTGGGGCAGCCCCATGGTGGTGGCTGGGGACAG
 CCTCATGGTGGTGGCTGGGGTCAAGGAGGTGGCACCCACAGTCAGTGAACAAGCCGAGTAAGCCAAAA
 ACCAACATGAAGCACATGGCTGGTGGCTGCAGCAGCTGGGGCAGTGGTGGGGGCCCTTGGCGGCTACATG
 CTGGGAAGTGCCATGAGCAGGCCCATCATACTTTCGGCAGTGACTATGAGGACCGTTACTATCGTGAA
 AACATGCACCGTTACCCCAACCAAGTGTACTACAGGCCCATGGATGAGTACAGCAACCAGAACAATTT
 GTGCAGACTGCGTCAATATCACAATCAAGCAGCACACGGTCACCACAACCACCAAGGGGGAGAATTC
 ACCGAGACCGACGTTAAGATGATGGAGCGCGTGGTTGAGCAGATGTGTATCACCAGTACGAGAGGGAA
 TCTCAGGCCATTACCAGAGGATCGAGCATGGTCTCTTCTCCTCTCCACCTGTGATCCTCCTGATC
 TCTTTCCTCATCTTCTCGATAGTGGGATGA

Figure S6. The human PrP gene has four upstream open reading frames (uORFs) in its 5' UTR, which may prevent translational repression of PrP by high levels of eIF2 α -P. ATGs (highlighted) and the resultant uORFs are shown for each one (solid coloured lines). 5' untranslated region (UTR) sequence is in black, coding sequence is shown in green. eIF2 α phosphorylation determines the concentration of ternary complex and consequently the rate of translation initiation. When eIF2 α -P levels are low, ternary complex concentration is high and normal mRNA transcripts with short 5' UTRs are translated with high efficiency. However, transcripts like *ATF4*^{1,2}, *BACE1*³ and *PrP* (above) with long, uORF-containing, secondary structure-rich 5' UTRs are inefficiently translated. When eIF2 α -P levels are high, under ER stress conditions, the translation of normal mRNA transcripts is inhibited as for *SNAP25*, *PSD95*, *β -actin*, while transcripts with long, uORF-containing, structured 5' UTRs are well known to be translated with increased efficiency (de-repression) under these conditions. See Sonenberg and Hinnebusch, Cell, 2009 for review⁴.

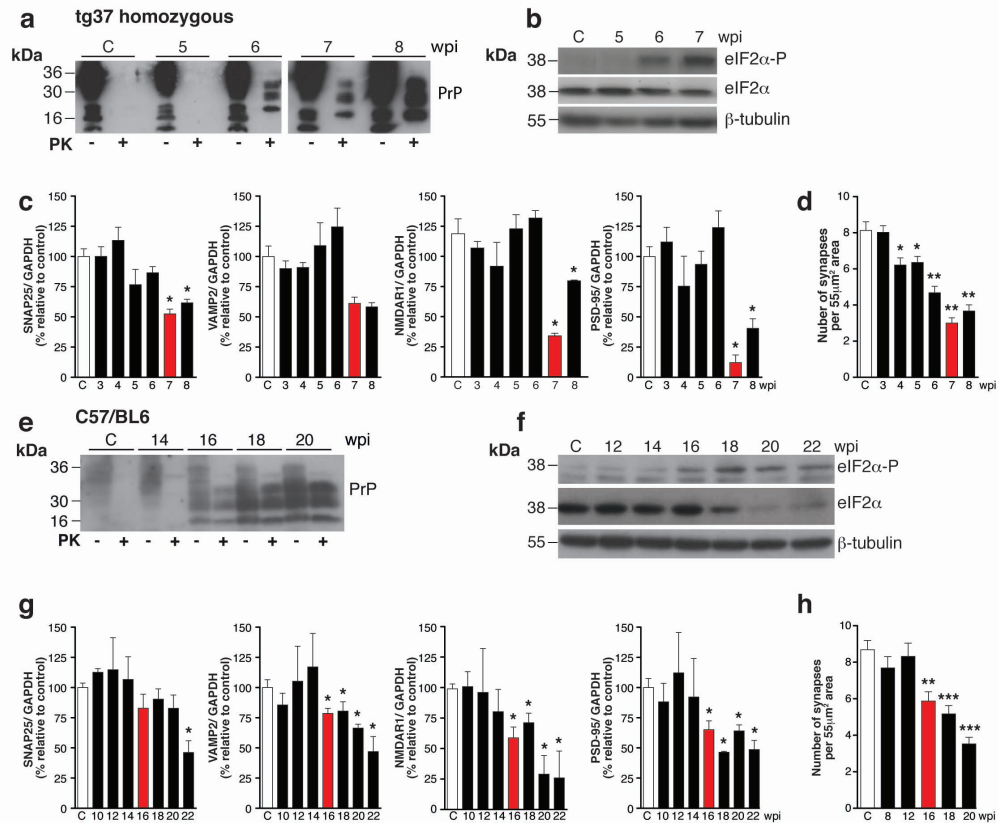


Figure S7. Onset of eIF2α phosphorylation and eIF2α-P-mediated translational repression correlates with levels of PrP in different lines of mice. a-d: Homozygous tg37 mice, in which mouse PrP is expressed at approximately six times wild type levels. **a**, Levels of total PrP rise during disease and protease resistant PrP^{Sc} is first detected at 6 w.p.i. **b**, eIF2α-P is first detected at 6 w.p.i., and **c**, levels of synaptic proteins SNAP25, VAMP2, NMDAR1 and PSD-95 decrease abruptly and significantly after 6 w.p.i. **d**, Synapse number declines from 4 w.p.i. and further decreases after 6 w.p.i. Mice are prion sick at 8 w.p.i. **e-h:** C57/BL6 mice, that express PrP at 1x wild type levels. **e**, Levels of total PrP rise during disease and protease resistant PrP^{Sc} is first detected at 16 w.p.i. **f**, eIF2α-P is detected at 16 w.p.i. when synaptic protein levels decline significantly, **g**, as does synapse number, **h**. Mice are prion sick at 22 w.p.i. For all experiments n = 3 mice, data in bar charts represents mean ± s.e.m. One-way ANOVA with Tukey's post test was used for multiple comparisons; $p < 0.05^*$; $p < 0.005^{**}$; $p < 0.0001^{***}$. Control mice were injected with normal brain homogenate (NBH) and examined at each time point. Data from all control groups was averaged to simplify figures for western blots. Representative blots and electron microscopy bar charts control samples are from 8 w.p.i. for tg37 homozygous mice and 20 w.p.i. for C57/BL6 mice.

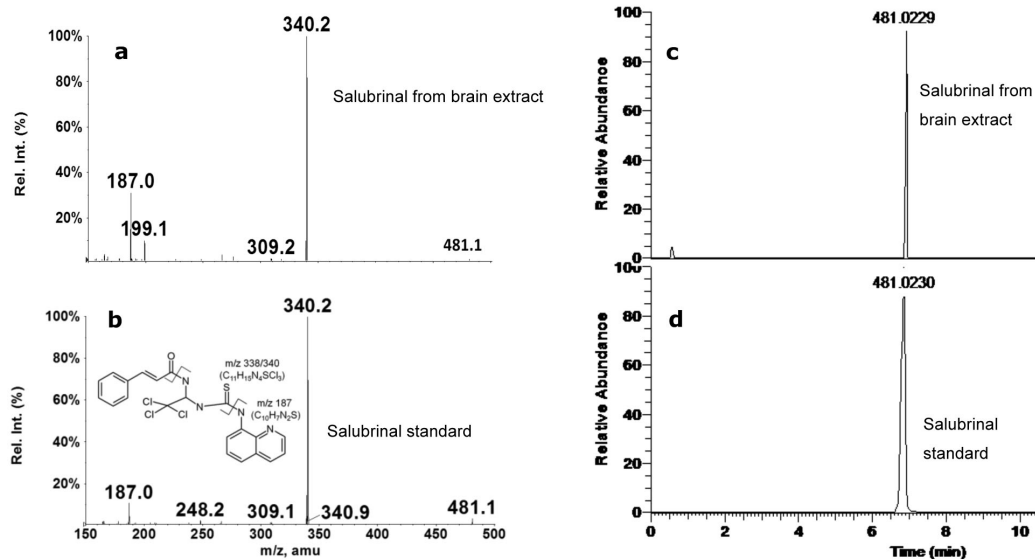


Figure S8. LC-MS confirmation of salubrial in mouse brain tissue following intraperitoneal administration. The MS product ion spectrum of the salubrial extracted from mouse brain tissue **a**, matched with that of authentic salubrial **b**, providing confirmation of the presence of salubrial in mouse brain. LC-MS extracted ion chromatogram confirmed the presence of the salubrial $[M+H]^+$ ions in mouse brain extract 2 hours after salubrial administration **c**, and this matched with the retention time and exact mass of a salubrial standard analysed under the same conditions **d**. The two main chlorine isotopes of salubrial were confirmed in brain: theoretical m/z 479.0261 and m/z 481.0232, found m/z 479.0251 (2 ppm) and m/z 481.0229 (0.6 ppm), respectively, with matching of all the main isotope peaks with standard salubrial. Measured salubrial concentrations at 2 hours after administration were 9.5 ± 1.9 pmol/g (wet weight) in brain tissue and 18 ± 2.8 nmol/L in blood plasma. Less than 1 pmol/g of salubrial was detectable at 24 hours in mouse brain or plasma.

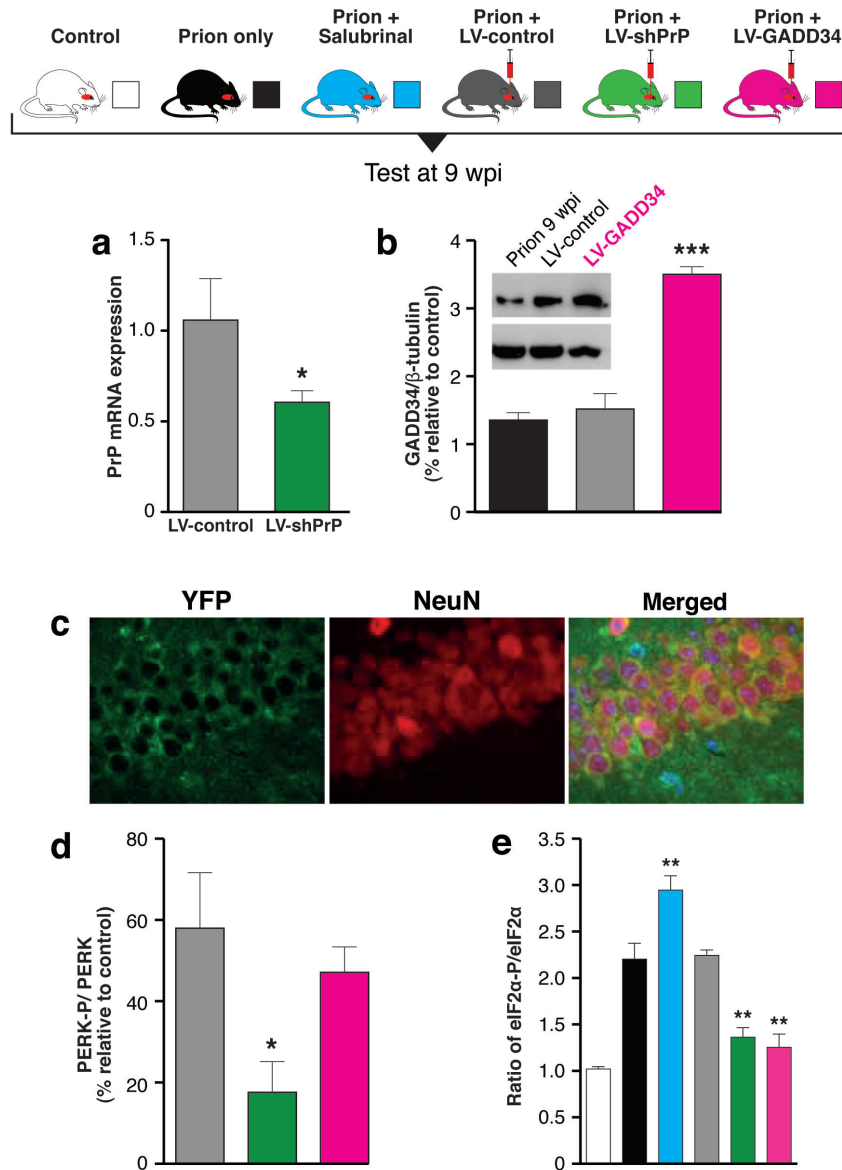


Figure S9. Confirmation of neuronal viral expression and quantification of PERK-P and eIF2 α -P in prion-infected mice. **a**, qPCR on RNA from whole hippocampi of LV-shPrP treated mice confirms knockdown of ~50% of PrP mRNA four weeks following LV-shPrP injection. **b**, LV-GADD34 expression is confirmed in hippocampi four weeks after LV-GADD34 injection by western blot for GADD34 and quantification (bar chart). **c**, Neuronal expression is confirmed in CA1 neurons by immunostaining for virally-expressed YFP (green) and the neuronal marker, NeuN (red). **d**, LV-shPrP reduces PERK-P in prion-infected mice. **e**, Both LV-shPrP and LV-GADD34 reduce eIF2 α -P levels in prion infected mice, while salubrinal treatment increases this. For all experiments $n = 3$ mice. Data in bar charts represents mean \pm s.e.m. One-way ANOVA with Tukey's post test was used for multiple comparisons; $p < 0.05^*$; $p < 0.005^{**}$; $p < 0.0001^{***}$. Control mice were injected with normal brain homogenate (NBH) and taken at 9 w.p.i. time point.

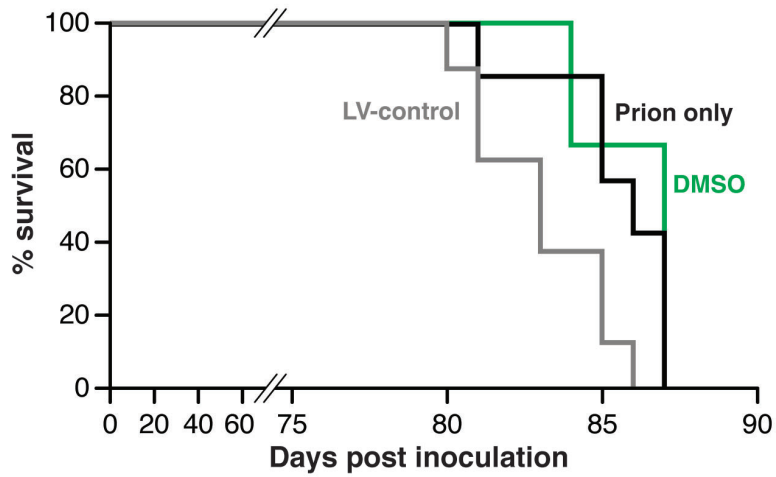


Figure S10. Kaplan Meier survival plots for prion infected control mice
Survival in LV-control treated (controls for LV-shPrP and LV-GADD34) and DMSO treated mice (controls for salubrinal treatment) is not significantly different from that of prion-only control mice.

Supplementary Methods

Real-time PCR (qPCR). RNA was extracted from hippocampi using the mirVANA RNA/miRNA isolation kit (Ambion, Inc), mRNA was reversed transcribed and semi-quantitative real-time PCR performed using sybr green supermix (Applied Biosystems). The following primers from mouse *PrP*, *ATF4*, *CHOP*, *SNAP25* and ribosomal protein-144 (*Rp144*) coding sequences were used:

(PrP) 5'- GAGCCAAGCAGACTATCAGTC -3'(forward), 5'- TCAGTCCACATAGTCACAAAGAG -3'(reverse);

(Rp144) 5'- GGCCGGTCTCTCGTTCTCA-3' (forward), 5'- TTACAGAAAGTCCTTCGGGTTTTT-3' (reverse);

(ATF4) 5'- TCGATGCTCTGTTTCGAATGG -3' (forward), 5'- CCAACGTGGTCAAGAGCTCAT-3' (reverse);

(CHOP) 5'- CACACGCACATCCCAAAGC -3' (forward), 5'- CCTGGGCCATAGAACTCTGACT -3' (reverse);

(SNAP25) 5'- GGCTGACCAGCTGGCTGAT-3' (forward) 5'- TGCCAGCATCTTTACTCTCTTCAA -3' (reverse);

(VAMP2) 5'- GCTGGATGACCGTGCAGAT -3' (forward) 5'- TGGCTGCACTTGTTTCAAAGT-3' (reverse);

(PSD-95) 5'- AGTCTGTGCGAGAGGTAG-3' (forward) 5'- GGATGAAGATGGCGATAGG-3' (reverse);

(NMDAR1) 5'-CGCGAGATCTCTGGGAAT -3' (forward) 5'- GACTCGTTCTTGCCGTTGATTA-3' (reverse).

Fold difference was analysed comparing either control (NBH) to prion samples or LV-control to LV-shPrP samples using the comparative Ct method⁵.

ER stress of HeLa cells. HeLa cells were treated with 2.5µg/ml tunicamycin for 0, 2, 5 or 10 hours and used as a positive control for ER stress for polysomal fraction analysis and immunoblots of the UPR pathway.

LC-Mass Spectrometry for analysis of salubrinal in brain tissue. Mice were injected with 1 mg/kg of salubrinal, control mice with diluted DMSO in saline (n=5 each group). After 2 and 24 hours blood plasma and whole brains were taken. Samples (200 mg) were extracted with chloroform:methanol (2:1), the solvent

evaporated to dryness and the dry residue redissolved in methanol before analysis. Salubrinal quantitative analysis (using external standards) was by LC-MS/MS (Applied Biosystems 4000 QTRAP) and accurate mass determination was by UPLC-MS (Thermo Scientific Orbitrap Exactive). LC conditions: 5 µl injection volume, Agilent SB C18 column (2.1 x 100 mm) or C18 Synergy Hydro (150 x 3 mm), water to-acetonitrile gradient modified with 0.1% formic acid. LC-MS/MS multiple reaction monitoring used precursor–product ion pairs of m/z 479.2>187.1 and m/z 481.2>187.1 in positive electrospray ionisation mode (ES⁺). Both isotopes were monitored. Accurate mass LC-MS used ES⁺ mode, scan range m/z 100 to 1200, a resolution of 25,000, ions acquired with and without applying parameters to induce collisional dissociation.

Immunocytochemistry for YFP expression. Lentivirally injected brains were paraffin embedded and immunostained for yellow fluorescent protein (YFP) using primary antibody anti-GFP, which detects YFP (1:500; Abcam), following antigen retrieval with sodium citrate. Sections were then incubated with secondary antibody Alexa-fluor-488 (1:500; Invitrogen) to visualize cells expressing YFP. Images were captured using a Zeiss Axiovert 200M microscope with a Colibri illumination system with Axiovision 4.8 software (Zeiss).

Supplementary references

- 1 Harding, H. P. *et al.* Regulated translation initiation controls stress-induced gene expression in mammalian cells. *Mol Cell* **6**, 1099-1108, (2000).
- 2 Spriggs, K. A., Bushell, M. & Willis, A. E. Translational regulation of gene expression during conditions of cell stress. *Mol Cell* **40**, 228-237, (2010).
- 3 O'Connor, T. *et al.* Phosphorylation of the translation initiation factor eIF2alpha increases BACE1 levels and promotes amyloidogenesis. *Neuron* **60**, 988-1009, (2008).
- 4 Sonenberg, N. & Hinnebusch, A. G. Regulation of translation initiation in eukaryotes: mechanisms and biological targets. *Cell* **136**, 731-745, (2009).
- 5 Schmittgen, T. D. & Livak, K. J. Analyzing real-time PCR data by the comparative C(T) method. *Nat Protoc* **3**, 1101-1108 (2008).